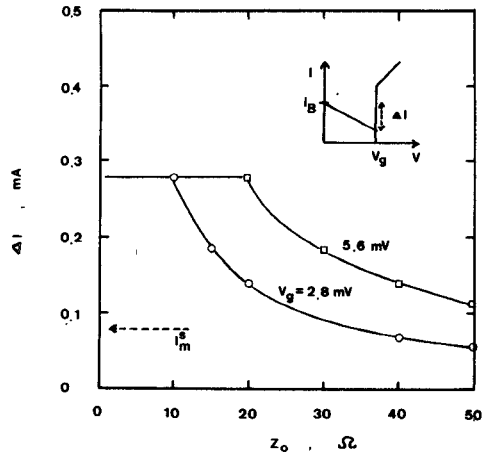

Fig. 7. Relationship between output currents ΔI and the characteristic impedance for Josephson packaging, where bias current I_B is 0.28 mA.

current I_m^s is about 0.08 mA for the case of a Josephson CIL receiver [4], considering the existence of thermal noise. When a higher characteristic impedance is used, the output voltage of the lead-alloy Josephson driver, with gap voltage $V_g = 2.8$ mV, is not sufficient, as shown in Fig. 7. It is necessary to use Josephson drivers which consist of higher gap energy superconductors such as NbN, or $2V_g$ operation drivers. For those drivers with high drivability, the limitation of the receiver sensitivity is not a serious problem. In particular, the device chips and packaging parts, which consist of the Nb–NbN/Nb_2O_5/NbN–Nb junction systems with $V_g = 4.2$ mV [18] and higher Z_0 Nb/NbN superconducting striplines with Nb ground planes, are preferable and can be practical in the near future from the viewpoints of low-noise electrical properties and reliable mechanical construction.

In order to realize large-scale superconducting systems, devices with high drivability, highly sensitive receivers, and high-impedance superconducting transmission lines are needed. When a higher impedance of $Z_0 = 40$–50 Ω is used in superconducting packaging, the matching capacitor does not play as important a role and should be omitted from the standpoint of decreasing crosstalk.

IV. Conclusion

The characteristic impedance influences of superconducting packaging systems (in particular, Josephson packaging) on fast switching signal propagation characteristics such as degraded switching time, amplitude distortions and crosstalk, signal propagation delay, and amplitude decay at the inductive and resistive connectors with matched capacitors were quantitatively evaluated for the first time by using the ASTAP computer simulation. The present choice of the characteristic impedance $Z_0 = 10$–12 Ω for a superconducting stripline is not adequate. The higher impedance of $Z_0 = 40$–50 Ω is useful from the standpoint of noise margin. A higher impedance choice makes ground connectors of the various connectors decrease, which is very useful for the large-scale package system.

In summary, in order to reduce amplitude distortions of transmitted ultrafast sig als in superconducting technology, it is important not only to educe the interconnection inductance values, but also to realize niform transmission superconducting lines with a higher characteristic impedance of $Z_0 = 40$–50 Ω, a highly sensitive superconductive receiver, and a superconducting driver with large drivability.

Acknowledgment

The authors would like to thank K. Aoki, Y. Tazoh, and K. Satoh for their valuable discussions in the initial stages of this study. They also wish to extend their gratitude to Dr. J. Matisoo for his valuable comments.

References

[1] R. L. Kautz, "Picosecond pulses on superconducting striplines," *J. Appl. Phys.*, vol. 49, pp. 308–314, Jan. 1978.
[2] W. Anacker, "Computing at 4 degrees Kelvin," *IEEE Spectrum*, pp 26–37, May 1979.
[3] H. C. Jones and D. J. Herrell, "The characteristics of chip-to-chip signal propagation in a package suitable for superconducting circuits," *IBM J. Res. Develop.*, vol 24, pp 172–177, Mar. 1980.
[4] M. Klein, "Chip-to-chip driver and receiver circuits for a Josephson computer," *IEEE J. Solid-State Circuits*, vol. SC-17, pp. 739–742, Aug. 1982.
[5] J. Temmyo and H. Yoshikiyo, "Numerical evaluation of lumped inductance influences of superconducting circuits interconnections on ultrafast switching signal propagation characteristics," *IEEE Trans. Microwave Theory Tech.*, vol. MTT-30, pp. 27–34, Jan. 1982.
[6] C J Anderson, M. Klein, and M. B. Ketchen, "Transmission of high speed electrical signals in a Josephson package," *IEEE Trans. Magn*, vol. MAG-19, pp. 1182–1185, May 1983.
[7] E. E. Davidson, "Electrical design of a high speed computer package," *IBM J. Res. Develop.*, vol. 26, pp. 349–361, May 1982.
[8] IBM Advanced Statistical Analysis Program, IBM Publ. No. SH20-1118, available through IBM branch office.
[9] C. Y. Ting, K. B. Grebe, and D. P. Waldman, "Controlled collapse reflow for Josephson chip bonding," in *Proc. Electrochemical Soc. Conf.*, May 1980, pp. 210–212.
[10] J. Temmyo, K. Aoki, H. Yoshikiyo, S. Tsurumi, and Y. Takeuchi," Solder bump height dependence of Josephson chip-to-card interconnection inductance using flip chip bonding technique," *J. Appl. Phys.*, vol. 54, pp. 5282–5286, Sept. 1983.
[11] K. R. Grebe, C. Y. Ting, and D. P. Waldman, "Orthogonal solder interconnections for Josephson packaging," in *Proc. Electrochemical Soc. Conf.*, May 1980, pp. 213–215.
[12] S. K. Lahiri, P. Geldermans, G. Kolb, J. Sokolowski, and M. J. Palmer, "Pluggable connectors for Josephson device packaging," in *Proc. Electrochemical Soc. Conf.*, May 1980, pp. 216–217.
[13] M. B. Ketchen *et al.*, "A Josephson system level experiment," *IEEE Electron Device Lett.*, vol. EDL-2, pp. 262–265, Oct. 1981.
[14] H. H. Zappe, "Josephson quantum interference computer devices," *IEEE Trans Magn.*, vol. MAG-13, pp. 41–47, Jan 1977.
[15] T. R. Gheewala, "A 30 ps Josephson current injection logic (CIL)," *IEEE Solid-State Circuits*, vol. SC-14, pp. 787–793, Oct. 1979.
[16] W. H. Chang, "The inductance of superconducting strip transmission line," *J. Appl. Phys.*, vol. 50, pp. 8129–8134, Dec. 1979
[17] W. H. Chang, "Measurement and calculation of Josephson junction device inductances," *J. Appl. Phys.*, vol. 52, pp. 1417–1426, Mar. 1981.
[18] A. Shoji, S. Kosaka, F. Shinoki, M. Aoyagi, and H. Hayakawa, "All refractory Josephson tunnel junctions fabricated by reactive ion etching," *IEEE Trans. Magn.*, vol. MAG-19, pp. 827–830, May 1983.

Calculation of High-Resolution SAR Distributions in Biological Bodies Using the FFT Algorithm and Conjugate Gradient Method

DAVID T. BORUP AND OM P. GANDHI, FELLOW, IEEE

Abstract—**A new method for the calculation of absorption in inhomogeneous, lossy dielectrics is presented. In this method, the convolutional nature of the electric-field integral equation is exploited by use of the FFT algorithms and the conjugate gradient method (CGM). The method is illustrated by solving for the SAR distribution for an anatomical cross section through the human eyes at 1 GHz.**

Manuscript received June 20, 1984; revised January 4, 1985. This work was supported in part by the NIEHS under Grant ES 02304.

The authors are with the Department of Electrical Engineering, University of Utah, Salt Lake City, Utah 84112.

0018-9480/85/0500-0417$01.00 ©1985 IEEE

I. Introduction

In a previous paper [1], a fast-Fourier-transform (FFT) method was presented for the calculation of high-resolution specific absorption rate (SAR) distributions in biological bodies. In that paper, the convolutional nature of the electric-field integral equation was exploited by use of the computationally efficient FFT algorithm and the method of steepest descent. The resulting numerical method for solving the matrix equation obtained by the method of moments was shown to be superior to matrix inversion, reducing the computation requirement from N^3 to $N \log_2(N)$ and the storage requirement from N^2 to N, where N is the number of unknown field sample points.

In this paper, an improvement in the method is made by replacing the steepest descent method with the conjugate gradient method (CGM), which converges more rapidly.

II. Implementation of the Method

The following discussion is a brief review of how the FFT method is implemented for the two-dimensional scalar problem of an arbitrary dielectric cylinder exposed to a transverse magnetic (TM) incident field.

As in Richmond [2], the two-dimensional electric-field integral equation is first discretized by the pulse basis. Then a linear system is arrived at by point matching. The resulting linear system is

$$E_z^i(n,m) = E_z(n,m) + \sum_i \sum_j (\epsilon_{ij} - 1) E_z(i,j) K(n,m,i,j) \tag{1}$$

where

$E_z^i(n,m)$ incident field at the center of pulse (n,m),
$E_z(n,m)$ total field at the center of pulse (n,m),
ϵ_{ij} complex relative permittivity of pulse (i,j)

and

$$K(n,m,i,j) = \frac{jk_0^2}{4} \iint_{s_{ij}} H_0^{(2)}(k_0 R_{nm})\, dx'\, dy'$$

where k_0 is the free-space propagation constant, s_{ij} is the surface of pulse (i,j), and

$$R_{nm} = \left((x_n - x') + (y_m - y')\right)^{1/2}.$$

In Richmond's method, the two-dimensional grid of sample points is linearly ordered to give a matrix equation which is then solved by matrix inversion. This requires computer storage proportional to N^2 and an amount of computation proportional to N^3.

However, if the discretization grid is rectangular and the x and y increments are constant, then K is a function of the shifts $(n-i)$ and $(m-j)$ only. In this case, the double sum in (1) is a two-dimensional discrete convolution. This allows the sum in (1) to be computed efficiently via the convolution theorem and the two-dimensional FFT algorithm. This approach requires storage proportional to N and an amount of computation proportional to $N \log_2(N)$.

This numerically efficient method for computing the forward matrix product (proportional to $N \log_2(N)$ versus N^2 for direct summation) suggests that the FFT algorithm can be used to implement any iterative matrix method that involves only forward matrix products. In addition, any iterative scheme that also requires the conjugate transpose operator can also be implemented since, if the linear operator A is defined by

$$Ax = x(n,m) + \sum_i \sum_j (\epsilon_{ij} - 1) x(i,j) K(n-i, m-j) \tag{2}$$

then the conjugate transpose operator A is given by

$$A^H x = x(n,m) + (\epsilon_{ij}^* - 1) \sum_i \sum_j x(i,j) K^*(n-i, m-j). \tag{3}$$

In particular, the method of steepest descent and the CGM described by Sarkar, Siarkiewitz, and Stratton [3] can be implemented in this way.

III. The Conjugate Gradient Method

The CGM, for the solution of $Ax = y$, is defined by

$$\begin{aligned}
&\boldsymbol{r}_0 = \boldsymbol{A}\boldsymbol{x}_0 - \boldsymbol{y} \\
&\boldsymbol{p}_0 = -A^H \boldsymbol{r}_0 \\
&\boldsymbol{x}_{n+1} = \boldsymbol{x}_n + t_n \boldsymbol{p}_n \qquad t_n = \|A^H \boldsymbol{r}_n\|^2 / \|A\boldsymbol{p}_n\|^2 \\
&\boldsymbol{r}_{n+1} = \boldsymbol{r}_n + t_n A \boldsymbol{p}_n \\
&\boldsymbol{p}_{n+1} = -A^H \boldsymbol{r}_n + q_n \boldsymbol{p}_n \qquad q_n = \|A^H \boldsymbol{r}_{n+1}\|^2 / \|A^H \boldsymbol{r}_n\|^2.
\end{aligned}$$

The asymptotic rate of convergence for the CGM is much faster than that of the method of steepest descent.

An important advantage of the CGM over other iterative methods such as the method of steepest descent is that the CGM is a finite step method. A finite step method is one which converges to the exact solution in a finite number of steps neglecting truncation and roundoff errors. The CGM is known to converge in a number of steps equal to the number of independent eigenvalues of the operator A. This is an advantage usually associated only with the direct methods such as Gaussian elimination.

The method further enjoys the advantage of an iterative method in that the truncation error does not accumulate but is limited to that incurred during the last iteration. This allows the CGM to succeed in cases where direct methods fail.

IV. Results

It was demonstrated in [1] that the FFT method yields excellent agreement with the analytic solutions for homogeneous and layered inhomogeneous circular cylinders. As a further example of the ability of the FFT method to handle electrically large two-dimensional TM problems, consider the anatomical cross section through the human eyes shown in Fig. 1.

The eight-tissue dielectric model was created from a published cross section [4] by an optical image digitizer. The problem was solved for a 1-GHz plane-wave incident field on an Eclipse microcomputer equipped with an array processor. Solution to a 10^{-3} residual magnitude required on the order of one hundred iterations, each iteration requiring about four minutes. Because the amount of core memory available was small, the FFT algorithm had to be decomposed by Singleton's algorithm [5]. This decomposition drastically increases the amount of disk transfer per iteration and accounts for the large amount of computer time needed. Solution on a larger computer capable of holding the entire FFT array in core would take much less time.

The SAR distribution obtained is shown in Fig. 2. Because of the small skin depth at this frequency, the absorption is mostly frontal, falling off exponentially toward the interior. An interesting feature of the distribution is the relatively high SAR (1.59×10^{-4} W/kg for $E_{inc} = 1$ V/m) at points A and B in the vitreous

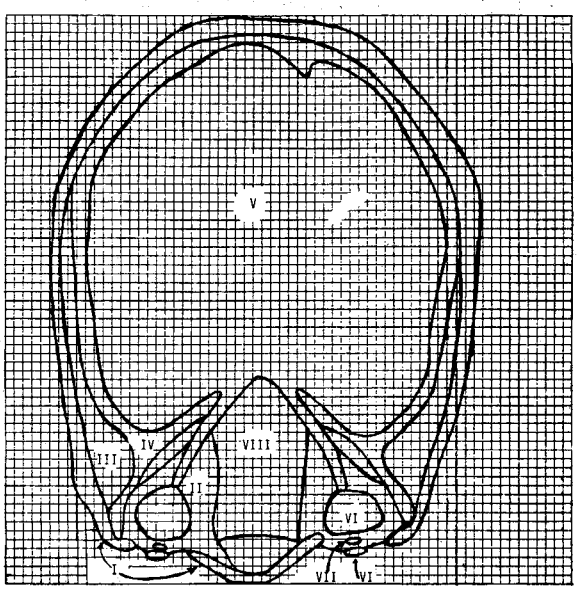

TISSUE	ϵ_r	σ
I. SKIN	44.5	1.01
II. FAT	6.4	0.12
III. MUSCLE	50.5	1.3
IV. BONE	6.4	0.12
V. BRAIN	48.0	1.25
VI. HUMOR	80.0	1.9
VII. LENS	50.5	1.3
VIII. NASAL	25	.6

64 x 64 = 4096 CELLS
FREQUENCY = 1 GHz
LENGTH = 20 cm
# NONZERO CELLS = 2600

Fig. 1. An eight-tissue model of a human cross section through the eyes. The dielectric values used were taken from [6].

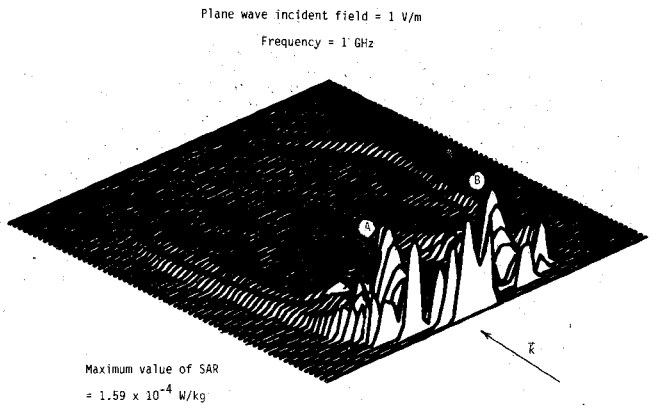

Fig. 2. Isometric plot of the FFT-calculated SAR distribution for the head cross section.

humor of the eyes. These peaks may be due to the fact that the size of the vitreous humor bodies are very close to one internal wavelength at this frequency.

The very shallow deposition at frequencies about 1 GHz may suggest the possibility of inhomogeneous modeling of only 2 to 3 skin depths into the body, reducing the number of unknowns drastically.

V. Conclusions

This paper illustrates the ability of the FFT method to obtain high-resolution SAR distributions for the two-dimensional TM absorption problem. Because the more general three-dimensional electric-field integral equation is also a convolution, it should be possible to extend the approach to the three-dimensional absorption problem.

References

[1] D. T. Borup and O. P. Gandhi, "Fast-Fourier-transform method for calculation of SAR distributions in finely discretized inhomogeneous models of biological bodies," *IEEE Trans. Microwave Theory Tech.*, vol. MTT-32, pp. 355–360, Apr. 1984.

[2] J. H. Richmond, "Scattering by a dielectric cylinder—TM case," *IEEE Trans. Antennas Propogat.*, vol. AP-13, pp. 334–341, Mar. 1965.

[3] T. K. Sarkar, K. Siarkiewicz, and R. Stratton, "A survey of numerical methods for solution of large systems of linear equations for electromagnetic field problems," *IEEE Trans. Antennas Propogat.*, vol. AP-29, pp. 847–856, Nov. 1981.

[4] A. C. Eycleshymer and D. M. Shoemaker, *A Cross Section Anatomy*. New York: D. Appleton, 1911.

[5] R. C. Singleton, "A method for computing the fast Fourier transform with auxiliary memory and limited high-speed storage," *IEEE Trans. Audio Electroacoust.*, vol. AU-17, pp. 91–97, June 1967.

[6] M. A. Stuchly and S. S. Stuchly, "Dielectric properties of biological substances—Tabulated," *J. Microwave Power*, vol. 15, pp. 19–26, 1980.

Characteristic Impedance of the Slab Line with an Anisotropic Dielectric

HISASHI SHIBATA, YUKIO KIKUCHI, AND RYUITI TERAKADO

***Abstract*—The characteristic impedance of the slab line with a circular conductor having an anisotropic dielectric is presented by using the affine and conformal transformations. Moreover, a simpler approximate formula of the impedance expressed in terms of $\epsilon_{\|}$, $\epsilon_{\perp}$, and r/h is also presented, where $\epsilon_{\|}$, $\epsilon_{\perp}$, r, and h are the principal axes–relative dielectric constants of the anisotropic dielectric, the inner conductor radius, and the half length between ground planes, respectively.**

I. Introduction

The slab line with a concentric circular conductor having an isotropic dielectric between parallel ground planes is used as the slotted section in microwave measurements and has been analyzed by many authors [1]–[5].

Due to the stability of its electrical properties, an anisotropic dielectric has been used in microwave integrated circuits. For various shielded striplines and covered microstrips, the analyses and some of the effects resulting from the utilization of an anisotropic dielectric have been reported [6]–[16].

This paper presents the characteristic impedance of the slab line with an anisotropic dielectric shown in Fig. 1. The permittivity tensor of the anisotropic dielectric in Fig. 1 is presented as

$$\bar{\epsilon}(x,y)=\begin{bmatrix}\epsilon_{\|} & 0\\ 0 & \epsilon_{\perp}\end{bmatrix}. \tag{1}$$

The application of the structure of Fig. 1 is not extensive. However, it is useful to analyze the line of Fig. 1 because it is a more general case than just including an isotropic dielectric.

It is useful to apply a transform method [6], [10] for the analysis of the slab line shown in Fig. 1. By the affine transfor-

Manuscript received June 21, 1984; revised December 18, 1984.

H. Shibata and Y. Kikuchi are with the Department of Electrical Engineering, Ibaraki College of Technology, Katsuta, Ibaraki, 312 Japan.

R. Terakado is with the Department of Electrical Engineering, Faculty of Engineering, Ibaraki University, Hitachi, Ibaraki, 316 Japan.

0018-9480/85/0500-0419$01.00 ©1985 IEEE